Draft version November 10, 2024
Typeset using LaTeX **twocolumn** style in AASTeX631

Orbit Determination for Asteroid 1990 UR1

Benti, K., Gupta, I., Lopez, E.[1]

[1]*Summer Science Program and Sommers-Bausch Observatory, University of Colorado Boulder, Boulder, CO, 80309, USA*

ABSTRACT

The orbit of asteroid 6485 Wendeesther (1990 UR1) is determined through a series of observations recording the right ascension (RA) and declination (DEC). Subsequently, its orbital elements that allow one to predict its short-term trajectory were determined using Python and the Method of Gauss. This is further refined with speed-of-light time correction. The uncertainties in the orbital elements were calculated by running the Monte Carlo simulation based on the standard deviation of the RA and DEC using the plate solved images from Astrometry.net. The orbital elements that were calculated and reported are the semi-major axis $a = 1.9097 \pm 0.0020$ *AU, eccentricity* $e = 0.167 \pm 0.0022$*, inclination* $i = 19.98 \pm 0.080^\circ$*, longitude of ascending node* $\Omega = 232.92 \pm 0.18^\circ$*, argument of perihelion* $\omega = 151.289 \pm 0.093^\circ$*, and mean anomaly* $M = 282.85 \pm 0.41^\circ$*.*

1. INTRODUCTION

The formation of the solar system occurred around 4.5 million years ago as a direct result of the impact of a supernova. This resulted in the collapse of interstellar dust and dense, gas-filled clouds and triggered the formation of a solar nebula whose gravitational force accreted matter and material. The large gravitational force as a result of the mass led to the creation of planets. Matter that was not large enough by mass formed comets, meteors, meteorites, and asteroids also characterised as space debris.

Asteroids are rocky remnants that orbit around the Sun. Most asteroids are found within the main asteroid belt- between Mars and Jupiter- and can be classified based on different factors, including composition and orbit type. The three different categories according to their composition are C-type, S-type, and M-type. C-type (Chondrite type) asteroids are the most commonly found within the main belt's outer region, are made up of clay/silicate rocks, and are amongst the oldest objects within the solar system. S-type (stony) asteroids are made up of nickel-iron/silicate materials and are most commonly found within the inner asteroid belt. M-type asteroids are metallic,vary in composition depending on their proximity to the Sun, and inhabit the main belt's middle region. Asteroids trajectories are often studied because of the potential threat they pose to life on Earth. Near Earth Asteroids are classified as asteroids who pass close to the Earth's orbit and pose a potential danger to life on Earth, as entry of them into the atmosphere would lead to global devastation. Earth would face the formidable consequences of acid rain, partial Sun blockage, as well as heated debris falling onto its surface. There are four types of Near Earth asteroids:

- Amor: asteroids with an orbit interior to Mars but entirely exterior to the Earth.
- Apollo: asteroids with longer semi-major axis than the Earth and crosses the orbit of the Earth.
- Aten: asteroids with shorter semi-major axis for their orbits compared to the Earth.
- Atira: asteroid with orbits always interior to the Earth's orbit.

Comets are frozen remnants from the creation of the solar system composed of ice, dust, and rocks. These are usually characterized by their long streaming tails caused by close orbit proximity to the Sun. The size of a comet varies depending on its position in relation to the Sun. Comets are a few to tens of miles large but average a center of about 6 miles. However, when a comet is closest in orbit to the sun it begins to vaporize and creates an atmosphere or a coma.

In addition to asteroids, meteoroids are masses composed of rock or iron and usually a by-product of debris from other space objects such as asteroids, comets, the Moon, and Mars. Some examples of their origins include collisions between two asteroids or the release of clouds of dust and debris as the comets pass the solar system. The collisions between asteroids can create a meteoroid with an orbit that might potentially lead it to

collide with other celestial bodies such as the Moon or Earth. Although meteoroids that enter Earth's atmosphere (meteors) typically disintegrate, if the meteoroid pass through, the impact of the explosion has a risk of causing shock waves that directly impact life on Earth. The possibility of such dangerous impact motivates the monitoring of space debris.

Asteroids can be further classified based on their peripheral planets. For instance, Mars-crossing asteroids intersect the orbit of Mars as they escape the Asteroid Belt located between Jupiter and Mars, likely becoming Near-Earth Asteroids (NEAs) in the future. These are often tracked with asteroid search campaigns such as *The International Astronomical Search Collaboration* and *Nasa's Jet Propulsion Laboratory*, which report the trajectories and current positions of near Earth and Mars-crossing asteroids. Using the data from those search campaigns, it is possible to determine the asteroid's future positions and therefore their potential threat to the Earth.

1990 UR1 is a Mars-crossing asteroid and its orbit can be described using its orbital elements: the semi-major axis, eccentricity, inclination, argument of perihelion, longitude of ascending node, and mean anomaly. Figure 1 gives a visual representation of the Orbital Elements.

The Method of Gauss is utilized to determine the orbit of the asteroid given its right ascension and declination on three different nights. Three observation nights were chosen out of the five in terms of the quality of the images, the uncertainties calculated from those observations and whether they are roughly equally spaced.

2. OBSERVATIONS AND IMAGE PROCESSING

2.1. *Data Acquisition*

The Sommers-Bausch Observatory (SBO, Minor Planet Centre Code 463) in University of Colorado Boulder hosts the Planewave 20- inch Artemis Telescope used to collect the data. The Observatory is located at 40.00371° N and 105.2630° W. This is a Corrected Dall-Kirkham (CDK) telescope of focal length 3454mm that minimises off-axis astigmatism and coma to enhance astroimaging and photography. This reflector telescope consists of two mirrors and a lens group, where the primary mirror is ellipsoidal and the secondary mirror is spherical. Table 1 above illustrates the observation

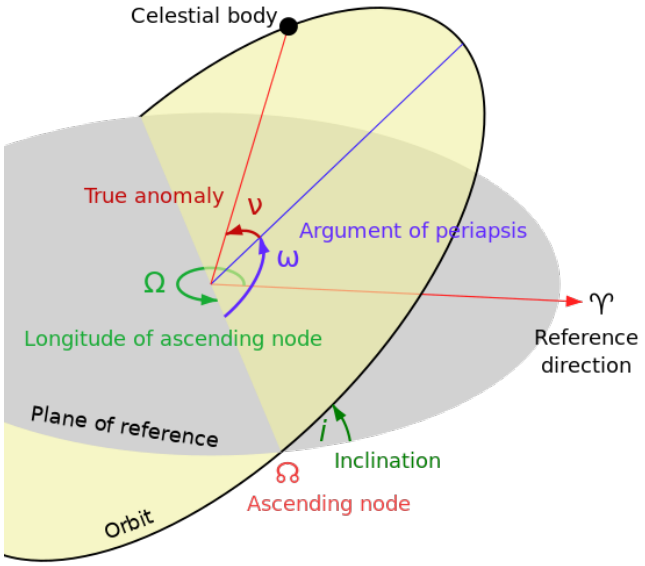

Figure 1. Orbital Elements

hours in UTC time, where *Artemis* is the name of the telescope used.

For capturing the asteroid, a Complementary Metal-Oxide Semiconductor (CMOS) imaging sensor is used, specifically the model ZWO ASI6200MM Pro with pixel array dimension 9576×6388 and pixel size of $3.76m$. This has a full-well capacity of $51.4ke$, quantum efficiency of 91% and read noise of $1.2e$ to $3.5e$. During observations, the telescope was cooled to approximately 0°C to minimise dark current.

To operate the telescope, TheSky, a software application on the deck that is connected to the telescope and allows the computer operations such as slewing to coordinates of the asteroid was used. During observations, 3 series of 3 repeats are taken at 10 minute intervals while maintaining the same field of view such that the asteroid moves relatively faster with respect to the celestial sphere for an Earth-based observer.
Throughout the observations, a variety of focus methods such as Bahtinov Masks and Autofocus settings are used to ensure precision and clarity of images. A UV/IR cutoff (L) filter is used, which focuses on enhancing the optical frequencies. A 30 second exposure is taken with a field of view of a 35.83 arcmin × 23.92 arcmin and 4x4 Binning. Given the asteroid's magnitude of 16.4, an exposure time of 30 seconds is used to ensure that enough photons are captured to detect and recognise the asteroid.

Table 1. Observation Journal

Date (DD/MM/YYYY	Time (UTC)	Location
23/06/2024	0600 - 0700	Artemis at SBO
25/06/2024	0600 - 0700	Artemis at SBO
04/07/2024	0600 - 0700	Artemis at SBO
10/07/2024	0600 - 0700	Artemis at SBO
13/07/2024	0600 - 0700	Artemis at SBO

2.2. *Image Reduction and Error Determination in Astrometry*

Multiple image series were taken as follows per observation times as recorded in Table 1:

- 10 Flats of exposure time 10 second to ensure count of 4000+ used to reduce dust and vignetting and subtract during stacking
- 10 Darks for Flats of exposure time 10 seconds and 10 Darks for Science Images to account for dark current i.e. thermal noise
- 3 sets of 3 Science Images at 10 minute intervals

Standard data reduction procedures were undertaken using DS9 and Astro Image J by stacking darks and flats onto the asteroid images i.e. science images such that the dark image counts are subtracted and then divided by flat image counts. In addition to the data reduction, Astrometry.net was used to plate solve the images of the asteroid and obtain x and y coordinates, the RA and DEC of the selected reference stars, and the x and y coordinates and RA and DEC for the asteroid. Using the data from the images, the Least Squares Plate Reduction (LSPR) algorithm was programmed to find the RA and DEC of the asteroid by creating best-fit line from the reference stars and finding the residuals by comparing the calculated value for the RA and DEC of the star with the predicted values from Astrometry.net. The standard deviation is also calculated using Eqn. (3) and (4).

$$residual_\alpha = \alpha_i - (b_1 + a_{11}x_i + a_{12}y_i) \quad (1)$$

$$residual_\delta = \delta_i - (b_1 + a_{21}x_i + a_{22}y_i) \quad (2)$$

$$\sigma_\alpha = \sqrt{\frac{\sum [residual_\alpha]^2}{N-3}} \quad (3)$$

$$\sigma_\delta = \sqrt{\frac{\sum [residual_\delta]^2}{N-3}} \quad (4)$$

where σ_α and σ_δ is the standard deviation of the RA and DEC, respectively. Eqn. (1) and (2) are the residuals for the RA and DEC, where b_1, a_{11}, a_{12}, b_2, a_{21}, and a_{22} are the best-fit plate coefficients. The asteroid's apparent magnitude (rmag) is further calculated through photometry as 6 stars with an rmag in the field of view are obtained from the UCAC4 Catalog in DS9. Using the apparent magnitudes and the Source-Sky of the stars obtained from Astro Image J, linear regression was performed to calculate the best-fit line. After the calculation, the rmag of the asteroid was calculated using the best-fit line and the asteroid's Source-Sky data from Astro Image J. Table 2 represents the asteroid's Right Ascension, Declination, their respective uncertainties and the apparent magnitude determined through photometry. Note that the date of observation is represented as YY/MM/DD.DDDDD and the uncertainties in the RA and DEC are only calculated for the middle observations for every observation night.

Table 2. Right Ascension and Declination Data from Observations

Date	Appr Mag	RA(°)	Uncertainty(°)	Dec(°)	Uncertainty(°)
2024/06/23.27552	16.0	286.71133	N/A	7.36392	N/A
2024/06/23.27590	16.0	286.71133	0.00017	7.36425	0.00014
2024/06/23.27629	16.2	286.71112	N/A	7.36425	N/A
2024/06/25.26640	15.7	286.16192	N/A	7.83911	N/A
2024/06/25.27126	15.7	286.15950	0.00017	7.84056	0.00014
2024/06/25.28033	15.8	286.15783	N/A	7.84244	N/A
2024/07/04.28200	16.4	283.47304	N/A	9.67822	N/A
2024/07/04.28235	16.4	283.47108	0.00014	9.67933	0.00011
2024/07/04.29096	16.3	283.47017	N/A	9.67969	N/A
2024/07/10.26147	16.2	281.61433	N/A	10.57189	N/A
2024/07/10.26887	16.3	281.61150	0.00017	10.57292	0.00014
2024/07/10.27496	15.8	281.60942	N/A	10.57325	N/A
2024/07/13.25033	17.0	280.69937	N/A	10.91308	N/A
2024/07/13.26054	16.0	280.69421	0.00012	10.91342	0.00015
2024/07/13.26620	15.8	280.69412	N/A	10.91336	N/A

3. ORBIT DETERMINATION

3.1. *Methods*

The **Gaussian Method** was used to determine the orbit of the asteroid. Given the RA and DEC from three nights of asteroid observations $(\alpha_1, \delta_1, t_1)$, $(\alpha_2, \delta_2, t_2)$, $(\alpha_3, \delta_3, t_3)$ and three Earth-Sun vectors ($\tilde{\mathbf{R}}$), the calculation of the position and velocity of the asteroid was done. Even though there was five observations, the three that were chosen produced clearer images and less uncertainties compared to the other observation nights. The three that were chosen are 04/07/2024, 10/07/2024, and 13/07/2024. Using the Earth and the Sun as a reference for the asteroid and calculating the vector extending from Earth to the asteroid, the range vector $\vec{\rho}$, the position $\vec{r}$ was calculated. Following the calculation of the position and velocity, the orbital element calculation for the the third chosen observation were done. For the orbital element computation, the position and velocity were converted from equatorial to ecliptic coordinates such that the orbital elements were computed in Python.

The following flowchart Figure 2 illustrates the overall experimental procedure throughout the experiment.

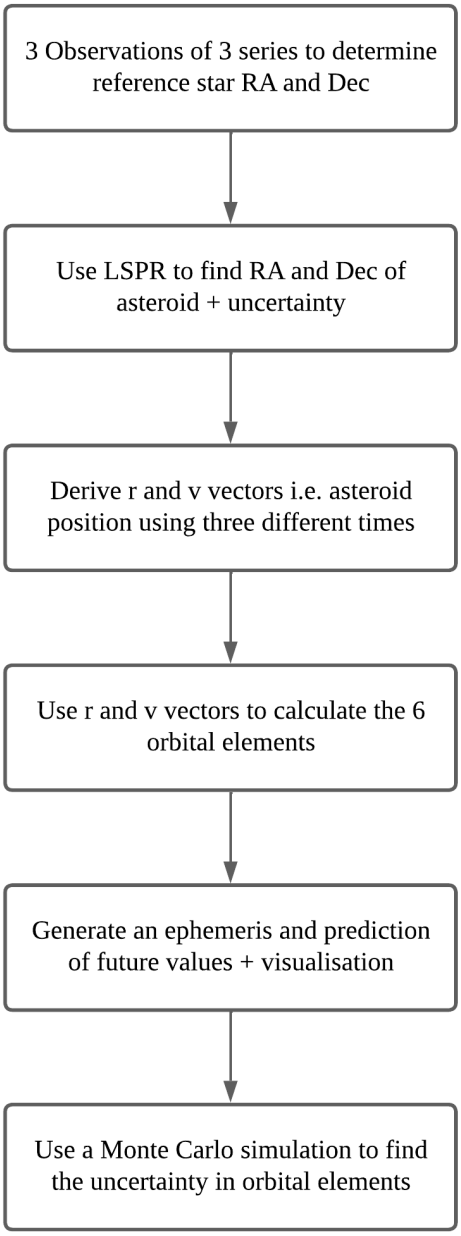

Figure 2. Steps for Orbit Determination

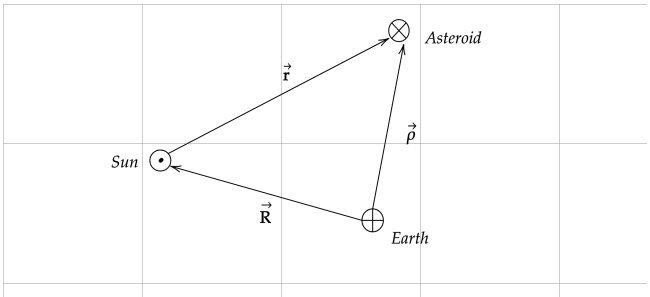

Figure 3. Sun, Earth, 1990 UR1 Asteroid vectors

To find the position of the asteroid with respect to the Sun,

$$\vec{r} = \rho\hat{\rho} - \vec{R} \quad (5)$$

The unit range vectors $\hat{\rho}$ for each observation were calculated using,

$$\hat{\rho} \; = \; < \cos\alpha\cos\delta, \;\; \sin\alpha\cos\delta, \;\; \cos\delta > \quad (6)$$

The values for the Earth-Sun vector, $\vec{R}$, were obtained from JPL Horizon Database for each observation.
Using the measured values of the RA and DEC for the

asteroid, $\hat{\rho}$ was calculated. To solve for the position of the second observation $\vec{r_2}$, the linear combination of the position for the first and third observation $\vec{r_1}, \vec{r_3}$ can be used.

$$\vec{r_2} = a_1\vec{r_1} + a_3\vec{r_3} \quad (7)$$

where a_1 and a_3 are constants.

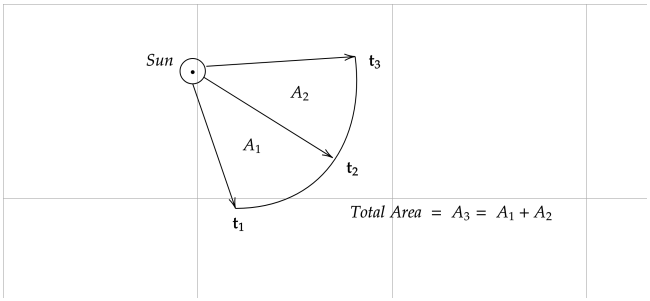

Figure 4. The orbit of the asteroid from time t_1 to t_3

According to Kepler's 2^{nd} law of planetary motion, the areas swept by the asteroid as it moves around the sun A in equal amount of time Δt are equal. The areas swept are also proportional to the change in position. As a result, an initial approximation for the constants a_1 and a_3 can be done using ratio of areas.

$$a_1 = \frac{A_2}{A_3} \approx \frac{t_3 - t_2}{t_3 - t_1} \quad (8)$$

$$a_3 = \frac{A_1}{A_3} \approx \frac{t_2 - t_1}{t_3 - t_1} \quad (9)$$

Using the values for a_1 and a_2 and plugging Eqn (1) into Eqn. (3),

$$\rho_2\hat{\rho_2} - \vec{R_2} = a_1\rho_1\hat{\rho_1} - \vec{R_1} + a_3\rho_3\hat{\rho_3} - \vec{R_3} \quad (10)$$

the magnitude of the range vector (ρ_1, ρ_2, ρ_3) were calculated. Following that, the position at the middle observation $\vec{r_2}$ was calculated using Eqn. (1).

However, this calculation gives as an inaccurate value for the position as it was dependent on the crude approximation of a_1 and a_3. The Taylor series expansion was used to get an accurate value for the position vector, that can be represented as,

$$\vec{r}(t) = \vec{r_0} + \dot{\vec{r_0}}t + \ddot{\vec{r_0}}\frac{t^2}{2} + \dddot{\vec{r_0}}\frac{t^3}{6} + ... \quad (11)$$

where $\vec{r_0}$, $\dot{\vec{r_0}}$, $\ddot{\vec{r_0}}$ are the intial position, velocity and acceleration of the asteroid at the middle observation, respectively

According to Newton's Laws of Motion and centripetal force from the Sun, the acceleration $\ddot{\vec{r}}_0$ is

$$\ddot{\vec{r_0}} = -\mu\frac{\vec{r_0}}{r_0^3} \quad (12)$$

and, the third derivative $\dddot{\vec{r_0}}$,

$$\dddot{\vec{r_0}} = -\mu(\frac{r_0^2\dot{\vec{r_0}} - 3(\vec{r_0}\cdot\dot{\vec{r_0}})\vec{r_0}}{r_0^5}) \quad (13)$$

where $\mu = GM_{sun}$. The $\vec{r}(t)$ can also be represented by regrouping the terms as,

$$\vec{r}(t) = [1-\mu\frac{t^2}{2r_0^3} + \frac{\mu(\vec{r_0}\cdot\dot{\vec{r_0}})t^3}{2r_0^5}]\vec{r_0} + (t - \frac{\mu t^3}{6r_0^3})\dot{\vec{r_0}} + ... \quad (14)$$

This can be expressed as,

$$\vec{r}(t) = f\vec{r_0} + g\dot{\vec{r_0}} \quad (15)$$

where $f = 1 - \mu\frac{t^2}{2r_0^3} + \frac{\mu(\vec{r_0}\cdot\dot{\vec{r_0}})t^3}{2r_0^5}$ and $g = t - \frac{\mu t^3}{6r_0^3}$

To make the calculations more convenient, $\vec{r}(t)$ will be expressed in terms of Astronomical Units **AU** and **Gaussian days**, where $\mu = 1$ and t is expressed interms of τ.

$$\tau = k\Delta t \quad (16)$$

where $k = 0.0172020989484 \quad \frac{AU^{\frac{3}{2}}}{day}$

Using the positions $\vec{r}(\tau_3)$ and $\vec{r}(\tau_1)$ obtained from Eqn. (14), a refined value of a_1 and a_3 was calculated using Eqn. (3). the position $\vec{r_2}$ was calculated through an iterative process, refining the a_1 and a_3 values throughout each iteration in the orbit determination code until the relative difference is less than 10^{-10}.

To get an even more close approximation for the position vector, correction for the speed of light travel time was done.

$$t_{corrected} = t_{observed} - \frac{\rho}{c} \quad (18)$$

, where c is the speed of light $c = 173.144643267\frac{AU}{solar\ days}$ As their is a factor of $\frac{\rho}{c}$ delay for the light to travel from the asteroid position to Earth, accounting for this will help refine the value of the position and velocity of the asteroid.

After obtaining the position and velocity $\vec{r}$ and $\dot{\vec{r}}$ of the asteriod, the orbital elements were calculated.

For these calculations, $\mu = GM = 1$, if time is measured

in Gaussian days and distance in **AU**.
To calculate the semi-major axis a,

$$a = \frac{1}{(\frac{2}{r} - \frac{v^2}{\mu})} \quad (19)$$

where $r = |\vec{r}|$ and $v^2 = \dot{\vec{r}} \cdot \dot{\vec{r}}$ and a is measured **AU**.
To calculate the eccentricity e,

$$e = \sqrt{1 - \frac{h^2}{\mu a}} \quad (20)$$

where $\vec{h} = \vec{r} \times \dot{\vec{r}}$
For calculating the inclination i,

$$\tan i = \frac{\sqrt{h_x^2 + h_y^2}}{h_z} \quad (21)$$

where h_x, h_y and h_z are the components of $\vec{h}$ and i is measured degrees. For certain values, quadrant checks are required, hence necessitating the need for sine and cosine values since they have a wide range. For the longitude of ascending node Ω,

$$\sin\Omega = \frac{h_x}{h \sin i} \quad \& \quad \cos\Omega = \frac{-h_y}{h \sin i} \quad (22)$$

The argument of perihelion is calculated using ω,

$$\omega = U - \nu \quad (23)$$

$$\sin U = \frac{z}{r \sin i} \quad \& \quad \cos U = \frac{x\cos\Omega + y \sin\Omega}{r} \quad (24)$$

$$\cos\nu = \frac{1}{e}[\frac{a(1-e^2)}{r} - 1] \quad \& \quad \sin\nu = \frac{a(1-e^2)}{h}\frac{\vec{r}\cdot\dot{\vec{r}}}{r} \quad (25)$$

where U is the true longitude, ν is the true anomaly and $h = |\vec{h}|$ and ω is measured in degree.

To calculate the Mean anomaly M,

$$M = E - e \sin E \quad (26)$$

$$\cos E = \frac{ae + r\cos\nu}{a} \quad \& \quad \sin E = \frac{r \sin\nu}{a\sqrt{1-e^2}} \quad (27)$$

where E is the eccentric anomaly and M is measured in degrees.

The Monte Carlo Simulation was used to calculate the uncertainties in the orbital elements of the asteroid using numerical error propagation from the errors in the three observations $\Delta RA_1, \Delta RA_2, ...$ and $\Delta DEC_1 \Delta DEC_2, ...$

The uncertainties in the RA and DEC for each of the observations are calculated from the *corr.fits* file obtained by plate solving our images through Astrometry.net.

Assuming the uncertainties in the RA and DEC follow a Gaussian distribution, the RA and DEC for each observation around the uncertainties is normalized, using

```
numpy.random.normal(center, sigma, size)
```

where *center* is the RA or DEC for each observation ,*sigma* the uncertainties associated with the RA or DEC and *size* determines the size of the array returned. After returning a series of RA and DEC for each observation, the orbit determination was run using the array of RA and DEC obtained 10^5 simulation was run to get a refined distribution for the orbital elements of the asteroid. Using the array of refined distribution of orbital elements, the mean and standard deviation σ for each orbital element is calculated.

After calculating the orbital elements, an ephemeris generation Python program was used to calculate the RA and DEC for the time of the third observation and do a comparison with the RA and DEC obtained during observation as in Table 3.

Table 3. RA and DEC of Asteroid 1990 UR1

	RA	DEC
Calculated	18:42:46.61	10:54:48.3
Observation	18:42:46.61	10:54:48.3

3.2. *Results*

Comparing the calculated value from the ephemeris generation program and observation, the relative difference is very negligible. Table 3 as follows illustrates the final values from the participant's Orbit Determination Code in addition to their uncertainty from the Monte Carlo simulation such that:

a = semi-major axis
e = eccentricity
i = inclination
Ω = longitude of ascending node
ω = argument of perihelion
M = mean anomaly

Table 4. Orbital Elements

Elements(Units)	Gupta	Benti	Lopez	Uncertainty
a(AU)	1.9097	1.9097	1.9097	0.0020
e	0.1667	0.1667	0.1667	0.0022
i(°)	19.976	19.976	19.976	0.080
Ω(°)	232.92	232.92	232.92	0.18
ω(°)	151.287	151.289	151.286	0.093
M(°)	282.85	282.85	282.85	0.41

3.2.1. *Asteroid's H Magnitude*

The H magnitude is the asteroids magnitude at zero phase angle as well as at geocentric and heliocentric distances. Based on the data from July 12 2024 06:00 UTC,
r = 1.901721 AU
Δ = 0.974019 AU
Apparent Magnitude V = 16.369
Phase angle $\alpha = 17.5699°$

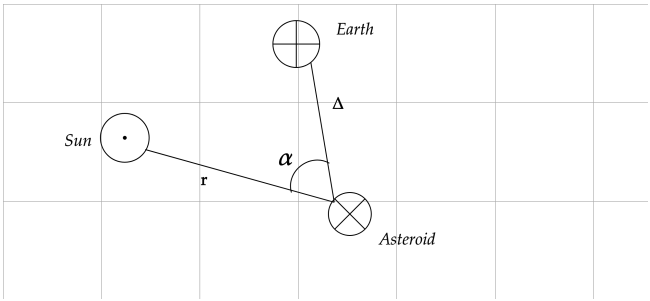

Figure 5. Determining the H magnitude

$$H(\alpha) = V - 5log(r\Delta) \quad (25)$$

$$H = H(\alpha) + 2.5log((1-G)\phi_1(\alpha) + G\phi_2(\alpha) \quad (26)$$

$$\phi_i = e^{-A_i(\tan\frac{1}{2}\alpha)^{B}i} \quad (27)$$

where $i = 1$ or 2, $A_1 = 3.33$, $A_2 = 1.87$, $B_1 = 0.63$ and $B_2 = 1.22$ and α is the phase angle in degrees. Using the Eqn. (25), (26) and (27) and the values for r, Δ, V, α, the H magnitude was calculated,

$$H = 14.11 \pm 0.5$$

3.2.2. *Probability Distribution of Orbital Elements*

The histograms in Figure 5 illustrate the probability distribution calculated by the Monte Carlo simulation for each orbital element.

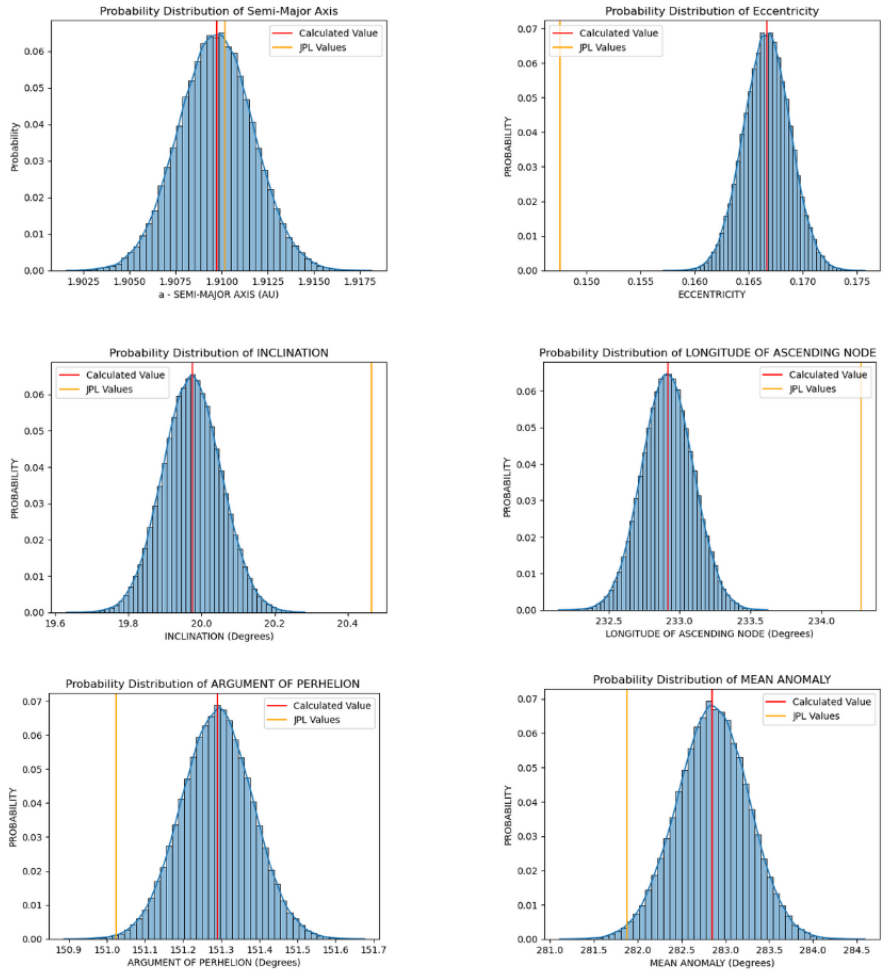

Figure 6. Probability Distribution of Orbital Elements

3.2.3. *Visual Orbit Plot*

The following diagram illustrates the asteroid 1990 UR1's trajectory in the solar system where the orange sphere represents the Sun, the blue represents the Earth's orbit and the red trajectory represents that of Mars. From this diagram, it is evident that the orbit is inclined with respect to the ecliptic and is a Mars-crossing asteroid. This corroborates with the research and observations and reflects the calculated orbital elements such as a semi-major axis of 1.9AU and eccentricity of 0.167.

To create this, the 3D function of Desmos was used to conduct matrix transformations with the inclination, longitude of ascending node, and argument of perihelion to convert the coordinate system to match the plane.

This is represented as follows:

$$\begin{pmatrix} cos(\Omega) & -sin(\Omega) & 0 \\ sin(\Omega) & cos(\Omega) & 0 \\ 0 & 0 & 1 \end{pmatrix} \begin{pmatrix} 1 & 0 & 0 \\ 0 & cos(i) & -sin(i) \\ 0 & sin(i) & cos(i) \end{pmatrix} \quad (28)$$

$$\begin{pmatrix} cos(\omega) & -sin(\omega) & 0 \\ sin(\omega) & cos(\omega) & 0 \\ 0 & 0 & 1 \end{pmatrix} \begin{pmatrix} x \\ y \\ z \end{pmatrix} \quad (29)$$

with all of the matrices multiplied to find the new coordinates. Subsequently, the semi-major and semi-minor axes were computed to substitute in an ellipse equation

where a is the semi-major axis and b is the semi-minor axis

$$\frac{x^2}{a^2} + \frac{y^2}{b^2} = 1 \quad (30)$$

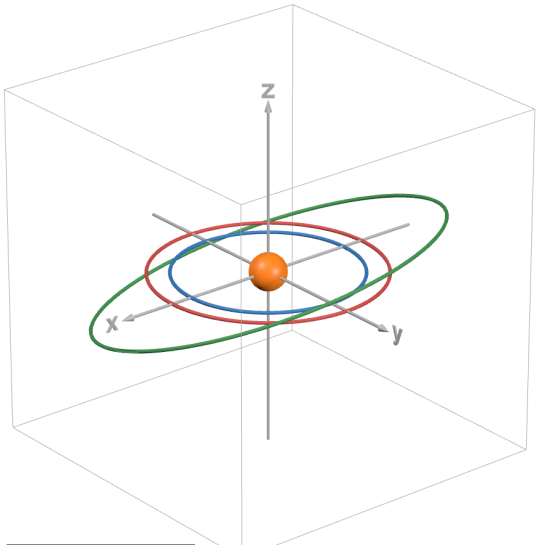

Figure 7. Asteroid Visualisation

4. DISCUSSION

The results for the orbital elements obtained using the observation data from five nights and the orbit determination and Monte Carlo simulation program had some difference as compared to the orbital elements listed for the asteroid, 1990 UR1, on JPL Horizons Database. Each calculated orbital element has some relative difference compared to the JPL values. The semi-major axis, a, was -0.024% different compared to JPL. The eccentricity, e, has a relative difference of 12.980%, which is the highest variation. The inclination i and the longitude of ascending node, Ω, have the relative difference of -2.386% and -0.580% compared to the JPL values, respectively. The Mean anomaly M was different from JPL values by 0.343%. Even though the relative differences of most of the orbital elements were small as compared to the JPL values, the eccentricity had a very noticeable there was a high Analyzing all the relative difference for each orbital element with respect to the JPL values shows that JPL values and the calculated values have some consistency with an overall small difference between them.

In addition, when performing the self-consistency check by recalculating the observed RA and DEC for the asteroid, 1990 UR1 using the Python ephemeris generation program, an RA and DEC were obtained with relative difference of 0.1%, which confirmed the calculations were consistent with the asteroid observation.

However, as with all observational astronomy, there are certain sources of error, both systematic and random. For instance, one approximation error is that the Taylor Series is upto the $4th$ term, which means that its accuracy can be improved with the addition of higher order terms in the Python Orbit Determination code. In addition, we focused on mitigating the time delay for the asteroid light to reach the Earth through light correction. This effectively means that the light that the telescope captures was that of the asteroid's previous position which may have changed.

While collecting data, our team collected dark and flat images for data reduction. One possible scope of improvement might be conducting bias subtraction with bias frames such that it reduces the noise pattern.

Additional correction that might have added more accuracy to the orbit determination is accounting for the stellar aberration. The calculation was made assuming that an image was taken standing still, which is an assumption to be corrected for as the observer moves due to Earth's rotation and orbit around the sun.

Some of the factors that affected the quality of the result for the asteroid might be systematic or instrumental errors that are inherent to the telescope used. Further study can be made using instruments with more accuracy to increase the quality of the data. In addition, the quality of the imaging might be affected by the weather or quality of the star at the day of the observation. For instance, as recorded in Table 2, the magnitude of the Asteroid in the 5^{th} observation fluctuated by a significant amount. This is likely a by-product of cloudy weather, which affected the observation times. In addition, certain exposures encountered difficulty in the photometry as a result of the Moon being extremely close to the asteroid, or one instance where the asteroid is almost indistinguishable from the star in one image. One possible improvement for better data collection might be delaying the observing times to a later time after midnight as the asteroid is closer to the meridian at that time. This further reduces the airmass and distortion in the images that affect the data collection and subsequent orbit determination.

5. REFLECTION

Kaku Benti: I had fun working on this research project. Tracing the asteroid orbit and determing the orbit was exciting and a huge learning opportunity. Collaborating with my team was also one of the best experiences as we worked together to achieve a common goal. I also had a fun experience coding my orbit determination code, applying my knowledge in physics, math and astronomy was exciting. Working with a team who wants to achieve their set goals and always open to learning new concepts, made me determined to contribute my best.

Eisha Lopez: The research experience of the project was extremely pleasurable and offered us a great learning experience. Being able to image the asteroid was always extremely exciting and tracking its movement over exposures was always a rewarding experience. Learning about orbital determination and having the opportunity to create a code that predicts the asteroids orbit was extremely fulfilling.

Ilisha Gupta: For me, my highlight throughout this project was being able to collaborate and meet new people who have a different skill set as we complemented each other's work. This was a really enriching summer as I was exposed to a variety of maths and physics, varying from the two-body problem, reduced mass, quantum mechanics, vector calculus, determinants and so much more. I really learnt a lot about myself and enjoyed the late nights tracking asteroids at 1 am. This summer improved my resilience and critical thinking as I solved a new variety of problems that required a unique approach, and was challenged with a variety of questions (such as the Question of the Days and the Professor's Challenge Problems). I hope to cherish these memories in the future, from the Game Nights to the cone theories and other classroom shenanigans.

Kaku Benti worked on the Methodology, Results and Discussion part of the report and generating the given data from our Python code. Ilisha Gupta wrote the Observation and Image Processing, and the Results section whilst processing the LaTeX format for tables and files. Eisha Lopez worked on the Introduction, Discussion, and References portion of the report. As a team, we collaborated well, both ON and OFF the deck as we took images and conducted the processing. We focused on splitting the work and continuously discussing work with each other such that we adapt based on everyone's workload and support each other.

6. ACKNOWLEDGEMENTS

We would like to thank Dr. Michael Dubson, Dr. Cassandra Fallscheer, Dr. Michael Rodruck,for their invaluable guidance and patience in teaching us about orbital determination. Their readiness to teach rendered an enjoyable learning experience. Additionally, we are sincerely grateful for our TAs Alan Tondryk, Emily Zhang, Kendra Nguyen, and Kevin Kim for their continued assistance in imaging the 1990 UR1 asteroid, debugging and supporting our theoretical understanding. A special thank you to the University of Colorado at Boulder for offering us the necessary means to conduct our research. Finally, we would especially like to thank the Summer Science Program for making this opportunity possible and ultimately for offering us a learning experience of a lifetime. Most importantly, this whole experience would be incomplete without our friends and peers at SSP who made the whole experience from the harsher aspects such as the late nights and relatively tight deadlines more manageable.

REFERENCES

[1]Debris of the solar system: Asteroids. ESA. (n.d.). https://www.esa.int/Science$_E$$xploration$/$Space_S$$cience$/$Rosetta$/$Debris_o$$f_t$$he_S$$olar_S$$ystem_A$$steroids$

[2]Meteoroid. Education. (n.d.). https://education.nationalgeographic.org/resource/meteoroid

[3]NASA. (n.d.-a). Asteroids: Facts - NASA science. NASA. https://science.nasa.gov/solar-system/asteroids/facts/

[4]NASA. (n.d.). Comets - NASA science. NASA. https://science.nasa.gov/solar-system/comets/

[5]NASA. (n.d.-b). Solar system: FACTS - NAS A science. NASA. https://science.nasa.gov/solar-system/solar-system-facts/

[6]NASA. (n.d.-d). Why study asteroids?. NASA. https://ssd.jpl.nasa.gov/sb/why$_a$$steroids.html$

[7]Optical design. PlaneWave Instruments. (n.d.). https://planewave.com/optical-design/

[8]Wendeesther. Asteroid Wendeesther — Space Reference. (n.d.). https://www.spacereference.org/asteroid/6485-wendeesther-1990-ur

[9]Why comets?. ESA. (n.d.-b). https://www.esa.int/Science$_E$$xploration$/$Space_S$$cience$/$Rosetta$/$Why_c$$omets$